Article

Synthesis of Au-Pd Bimetallic Nanoflowers for Catalytic Reduction of 4-Nitrophenol

Tao Ma, Feng Liang * [ID]**, Rongsheng Chen, Simin Liu** [ID] **and Haijun Zhang**

The State Key Laboratory of Refractories and Metallurgy, School of Chemistry & Chemical Engineering,
Wuhan University of Science and Technology, Wuhan 430081, China; mataowust@163.com (T.M.);
chenrs@wust.edu.cn (R.C.); liusimin@wust.edu.cn (S.L.); zhanghaijun@wust.edu.cn (H.Z.)
* Correspondence: feng_liang@whu.edu.cn; Tel.: +86-27-6886-2107

Abstract: Due to the great potential to improve catalytic performance, gold (Au) and palladium (Pd) bimetallic catalysts have prompted structure-controlled synthesis of Au-Pd nanoalloys bounded by high-index facets. In this work, we prepared Au-Pd bimetallic nanoflowers (NFs) with a uniform size, well-defined dendritic morphology, and homogeneous alloy structure in an aqueous solution by seed-mediated synthesis. The prepared bimetallic NFs were fully characterized using a combination of transmission electron microscopy, Ultraviolet-Visible (UV-vis) spectroscopy, inductively coupled plasma optical emission spectroscopy, and cyclic voltammetry measurements. The catalytic activities of the prepared Au-Pd nanoparticles for 4-nitrophenol reduction were also investigated, and the activities are in the order of Au@Pd NFs > Au-Pd NFs (Au_1Pd_1 core) > Au-Pd NFs (Au core), which could be related to the content and exposed different reactive surfaces of Pd in alloys. This result clearly demonstrates that the superior activities of Au-Pd alloy nanodendrites could be attributed to the synergy between Au and Pd in catalysts.

Keywords: bimetallic nanoparticles; Au-Pd alloy; reduction; 4-nitrophenol

1. Introduction

Since Haruta's seminal work [1,2], well-defined gold nanoparticles (AuNPs) have been developed to achieve chemical transformations, and can be applied in the manufacture of pharmaceuticals, fine chemicals, petroleum processing, and food additives under milder reaction conditions [3,4]. Recently, bimetallic nanoparticles, composed of two different metal elements, have received a great deal of attention, particularly in the field of catalysis, as they have often shown enhanced catalytic performance compared with their corresponding monometallic counterparts, due to alloy effects or synergistic effects [5–9]. Among the various alloy catalysts reported, gold (Au) and palladium (Pd) bimetallic nanoparticles are of particular interest because of their superior activity in low-temperature carbon monoxide oxidation, synthesis of vinyl acetate, direct H_2O_2 synthesis, hydrodechlorination of Cl-containing pollutants, hydrodesulfurization of S-containing organics, hydrogenation of hydrocarbons, acetylene trimerization, ethanol oxidation and many other reactions [10–12].

Recently, attention has also been focused on anisotropic branched metal nanoparticles that generally exhibit enhanced catalytic activity, which is attributed to their high surface to volume ratio and high-energy active center atoms located at the sharp tips with unsatisfied valency [13–16]. In our recent work, we synthesized multibranched gold nanostars by a seeded growth method. It was found that the gold nanostars presented better catalytic activity than gold nanocages and gold nanoantennas for the reduction of 4-nitrophenol (4-NP) to its amino derivative 4-aminophenol (4-AP) via sodium borohydride ($NaBH_4$) at room temperature [17]. As the degradation of 4-NP is an important reaction in fine chemicals and pharmaceuticals industries [18] and can be conveniently tracked by UV-vis

absorption spectroscopy, this reaction has been used to study the catalytic efficiency of numerous monometallic and alloy nanocatalysts of different sizes, shapes, and compositions [19].

In this work, we demonstrate that the seed-mediated synthesis of morphology-controlled Au-Pd bimetallic nanoparticles can be conveniently achieved. All resultant Au-Pd nanoflowers exhibited superior catalytic activity for the reduction of 4-nitrophenol as compared to monometallic Au nanoparticles in our lab, and the catalytic activity of the nanoparticles depended on the alloy composition.

2. Results and Discussion

2.1. Synthesis and Characterization of Au-Pd Nanoflowers

Although there are many routes toward controlling the size, shape, composition and architecture of bimetallic dendritic nanocrystals (e.g., highly branched nanocrystals, stars, and flowers, among others), including seed-mediated growth, galvanic replacement, anisotropic etching of nanocrystals, and aggregation or oriented attachment [8], seed-mediated reduction is the most straightforward method for generating bimetallic nanocrystals [8,11]. Typically, seed-mediated growth requires two processes: (i) the reduction of a metal precursor to form seeds with uniform and relatively small sizes; and (ii) the reduction of another metal on the as-prepared seeds. Therefore, we firstly prepared gold nanospheres (Au core, ~16 nm) [17], gold and palladium bimetallic nanoparticles (Au_1Pd_1 core, ~ 20 nm) [20] and gold nanostars (~40 nm) [17,21] as seeds (Figure S1), then palladium was reduced and deposited on these seed nanocrystals, leading to the formation of three morphology-controlled Au-Pd nanoflowers (Scheme 1).
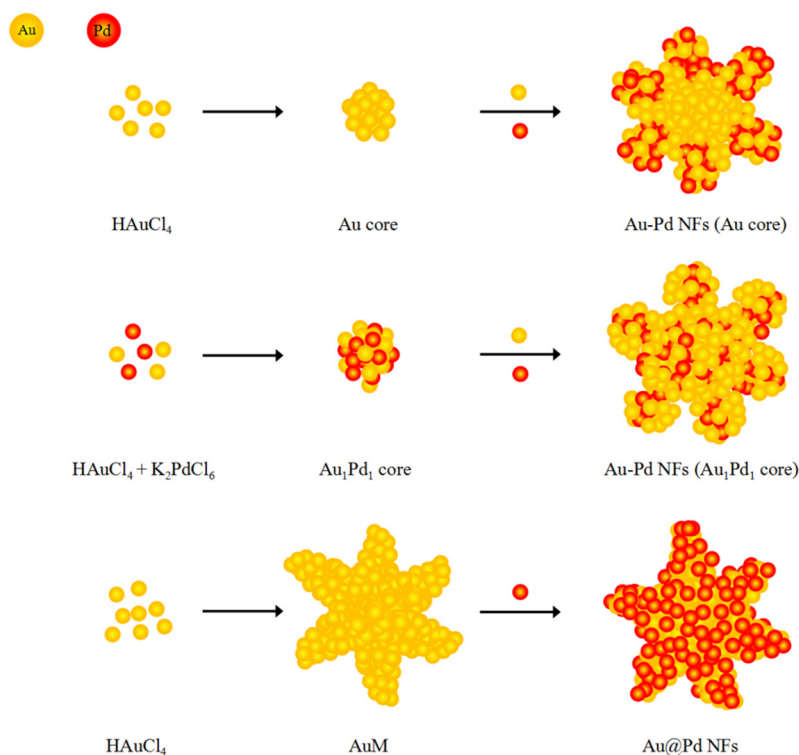
Scheme 1. Schematic illustration of the formation of three morphology-controlled Au-Pd nanoflowers (NFs) in this work by seed-mediated growth.

Two Au-Pd bimetallic nanoflowers (NFs) from gold nanosphere seed (Au core) and gold-palladium bimetallic seed (Au_1Pd_1 core) were synthesized by coreduction of $HAuCl_4$/K_2PdCl_6 mixtures with ascorbic acid in the presence of silver nitrate, the larger Au-Pd bimetallic nanoflowers

(Au@Pd NFs) from gold nanostar were synthesized by reduction of K_2PdCl_6 with ascorbic acid. Au-Pd NFs (Au core), Au-Pd NFs (Au_1Pd_1 core) and Au@Pd NFs all have dendritic shapes with a number of branches, and the average sizes obtained by measuring the length from one branch edge to another one on the opposite side are around 42, 39 and 62 nm respectively (Figure 1a–c).
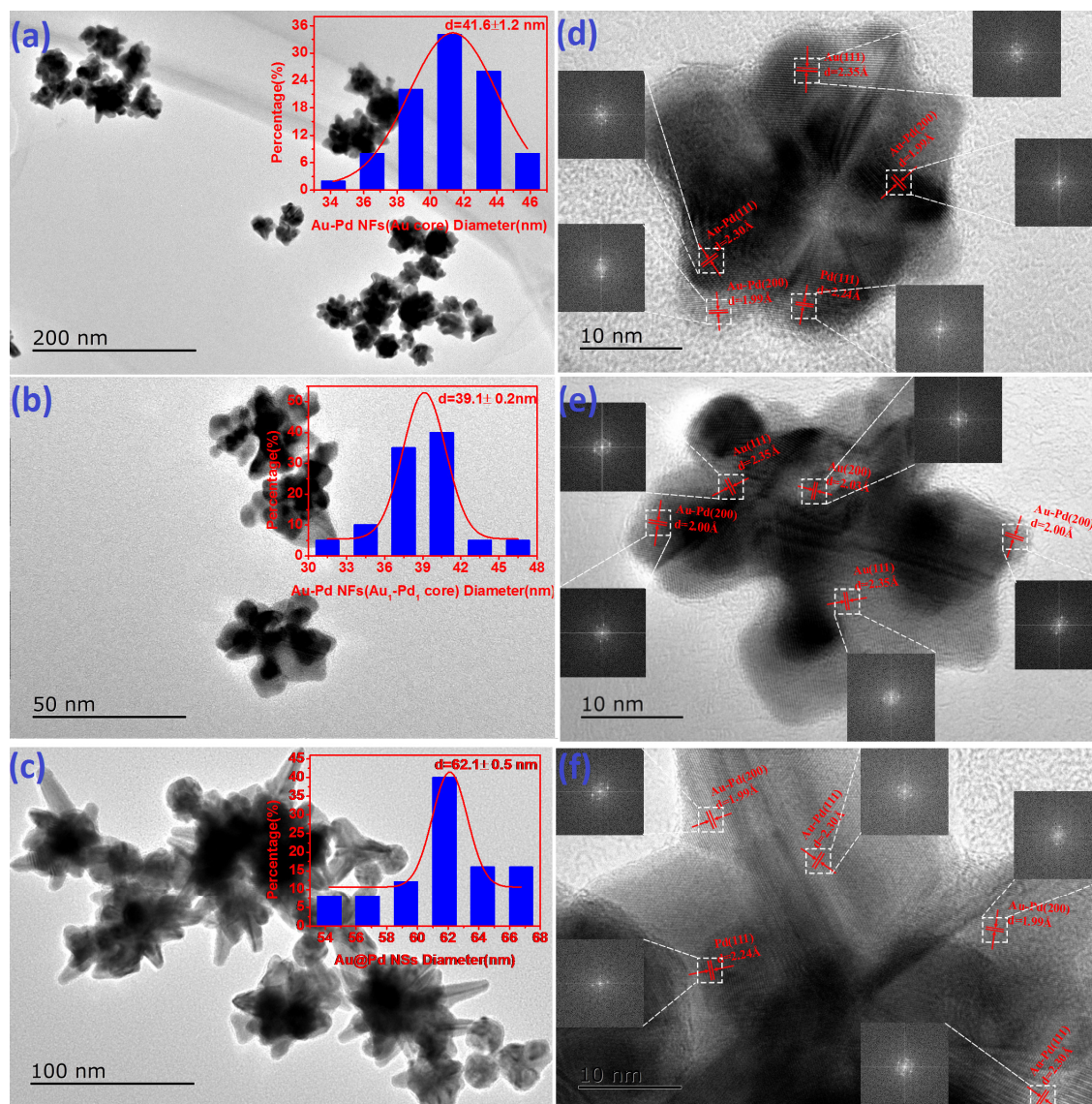

Figure 1. Typical transmission electron microscopy (TEM) images of synthesized nanoflowers in this work: (**a**) Au-Pd NFs (Au core); (**b**) Au-Pd NFs (Au_1Pd_1 core); (**c**) Au@Pd NFs; and high-resolution TEM image of (**d**) Au-Pd NFs (Au core); (**e**) Au-Pd NFs (Au_1Pd_1 core); (**f**) Au@Pd NFs, the insets indicate the corresponding fast Fourier transform (FFT) patterns obtained in the framed part (dashed line) in the panel. The microstructures were characterized by JEM-2010 UHR microscope (JEOL, Tokyo, Japan).

In order to verify the formation of the alloyed structure in the prepared NFs, the lattice fringes were further analyzed based on high-resolution transmission electron microscopy (HRTEM) images. The HRTEM images (Figure 1d) and corresponding fast Fourier transform (FFT) patterns (insets in Figure 1d) indicate that Au-Pd NFs (Au core) are obvious crystalline structures with well-defined lattice planes. Interplanar spacings corresponding to the {111} planes of pure metallic Au (JCPDS file number 04-0784) and pure metallic Pd (JCPDS file number 87-0638) were determined, and found to be 0.235 and 0.224 nm, respectively. The measured interplanar distances of Au-Pd NFs (0.230 and 0.199 nm)

show a lower value compared with the interplanar spacing of Au metallic ones, and a higher value compared with the interplanar spacing of Pd metallic ones: 0.235 nm (lattice spacing of Au {111} plane) > 0.230 nm > 0.224 nm (lattice spacing of Pd {111} plane) and 0.204 nm (lattice spacing of Au {200} plane) > 0.199 nm > 0.194 nm (lattice spacing of Pd {200} plane), which is evidence of the incorporation of Pd in the Au lattice [22–24]. The HRTEM images (Figure 1e,f) also exhibited the {111} or {200} planes of Au-Pd alloy, indicating the formation of the Au-Pd alloy phase in the Au-Pd NFs (Au_1Pd_1 core) and Au@Pd NFs because of the close matching between the lattice spacings of Au and Pd.

To further confirm the generation of Au-Pd alloy, elemental analyses were performed using inductively coupled plasma optical emission spectroscopy (ICP-OES, IRIS Advantage Duo ER/S spectrometer, Thermo Jarrell Ash, Franklin, MA, USA). Three nanoflower samples were suspended in freshly prepared aqua regia and heated until completely dissolved, and then diluted with double-distilled water [21]. Both Au and Pd elements were able to be detected in the three nanoflower samples, and the mass ratio of Au to Pd is 18:1, 17.6:1, 3.5:1 in Au-Pd NFs (Au core), Au-Pd NFs (Au_1Pd_1 core) and Au@Pd NFs, respectively. The synthesized nanoparticles were also characterized by UV-vis spectroscopy as supplement technique, surface plasmon resonance (SPR) peaks of Au-Pd NFs (Au core), Au-Pd NFs (Au_1Pd_1 core) and Au@Pd NFs were able to be detected at 633 nm, 685 nm and 695 nm, respectively (Figure 2), which is reasonable for Au-Pd bimetallic nanoparticles [25].
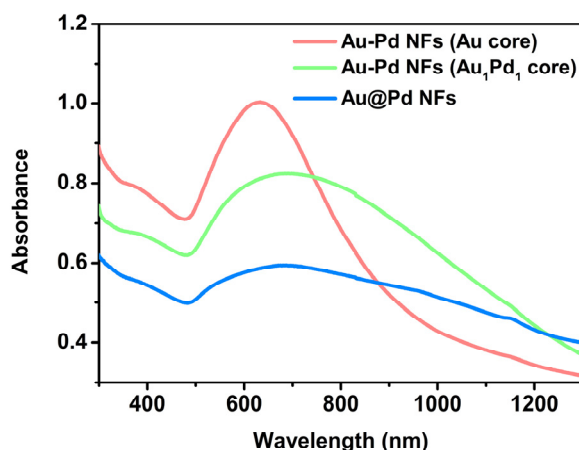

Figure 2. Typical UV-vis spectra of bimetallic nanoflowers solution in aqueous medium at room temperature. The absorption spectra were acquired with a UV-3600 UV-vis-NIR spectrometer (Shimadzu, Kyoto, Japan).

The cyclic voltammetry (CV) curves were also utilized to evaluate the different nanoparticles. Figure 3 reveals the voltammetric behaviors of Au-Pd nanoflowers in 0.5 M N_2-saturated H_2SO_4 solution [26]. In our case, a combination of the features of both metals was observed, i.e., a more pronounced Au oxide reduction peak around 1.2 V for Au-rich surfaces was observed, while a Pd oxide reduction peak around 0.7 V in the case of Pd-rich surfaces, was also observed [27,28]. The voltammetric features reinforce the earlier conclusions drawn from TEM analyses in Figure 1, and confirm the formation of alloys on the NF surface for the whole stoichiometry range of Au-Pd nanoparticles. From 0.1 to 0.6 V, a pair of well-defined anodic (cathodic) peaks attributed to hydrogen desorption (adsorption), which corresponds to the Pd surface on the alloy because of its unique function in absorption of hydrogen [29].
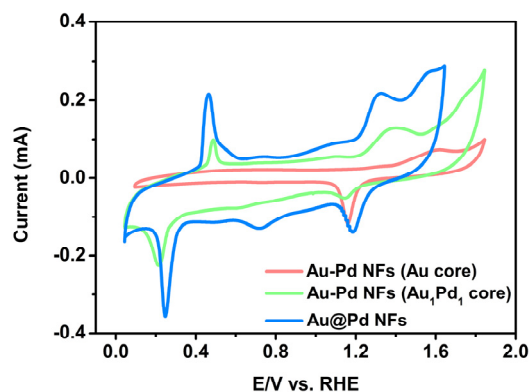
Figure 3. Cyclic Voltammetric (CV) responses (50 mV s^{-1}) for three nanoflowers in 0.5 M N$_2$-saturated H$_2$SO$_4$ solution up to 1.8 V vs. Reversible Hydrogen Electrode (RHE) and the saturated calomel electrode used as the reference electrode. CV curves were recorded on CHI660e electrochemical workstation (CH Instruments, Shanghai, China).

Moreover, it is curious why Au-Pd nanoflowers were produced in our seed-mediated synthesis. Typically, morphological change could be originally attributed to change in growth kinetics [8,11]. The formation of Au-Pd nanoalloy is based on the coreduction of a stepwise procedure of Pd (IV) to Pd(II) and Pd(II) to Pd(0), and Au(III) to Au(0). Although the PdCl$_6$$^{2-}$/PdCl$_4$$^{2-}$ reduction potential (1.288 V) is higher than that of AuCl$_4$$^-$/Au (1.002 V) and PdCl$_4$$^{2-}$/Pd (0.591 V), and thus possesses the priority of ascorbic acid reduction, the AuCl$_4$$^-$/Au and PdCl$_4$$^{2-}$/Pd conversions directly contribute to the formation of the Au-Pd nanoalloy. The relative high potential of AuCl$_4$$^-$/Au facilitates the deposition of Au atoms on the core in preference to Pd atoms. After AuCl$_4$$^-$ was consumed in the solution, the growth of Pd would arise. The further fusion and aggregation of Pd atoms with cores produces the flowerlike structure [8,11,28]. The higher reactivity of Au ions is proved by the inductively coupled plasma (ICP) measurement, which indicated that the Au to Pd mass ratio was able to reach 18:1. The fast mobility of Ag atoms relative to Au atoms, which could promote the random nucleation of Au atoms on the seed to produce the dendritic structure [30,31]. Similar to Au-Rh bimetallic nanoparticles [32,33], the surface free energy for Au is 1.63 J/m^2, whereas the corresponding value for Pd is 2.04 J/m^2 [34], which should favor the formation of thermodynamically favorable Au-shell Pd-core structures [35]. The enrichment of the surface with Au has been confirmed by ICP and CV measurements. However, understanding the relationships between reaction conditions and final nanostructures is challenging in our limited examples. A comprehensive examination of how various synthetic parameters influence the bimetallic nanostructure is required.

2.2. Catalytic Reduction of 4-Nitrophenol

Au-Pd NFs were also tested as catalysts for the reduction of 4-nitrophenol with NaBH$_4$, according to our reported procedures [17]. After the addition of NaBH$_4$, the predominant species 4-nitrophenolate ion is a strong visible absorber with a maximum absorbance at 400 nm. The reduction of 4-NP to 4-AP could be evidenced by a decrease of absorbance to 400 nm [19]. To compare the catalytic activities of NFs, we calculated the reaction rate constants by measuring the intensity (A) of the absorption peak at 400 nm with the reaction time and plotting ln(A_t/A_0) versus reaction time t. As shown in Figure 4a, the complete conversion of 4-NP takes less than 1 min. As shown in Figure 4b, a linear relationship between ln(A_t/A_0) and reaction time t was obtained for the three NF catalysts in the presence of excess NaBH$_4$. The rate constants (k_{app}), determined by the slopes of the lines, were 15.5, 9.33, and 2.8 min^{-1} for Au@Pd NSs, Au-Pd NFs (Au$_1$Pd$_1$ core) and Au-Pd NFs (Au core), respectively. This result demonstrates a clear dependence of activity on the chemical composition of NFs. We would also like to stress that our catalyst Au@Pd NS is more active than those reported in the literature [19].
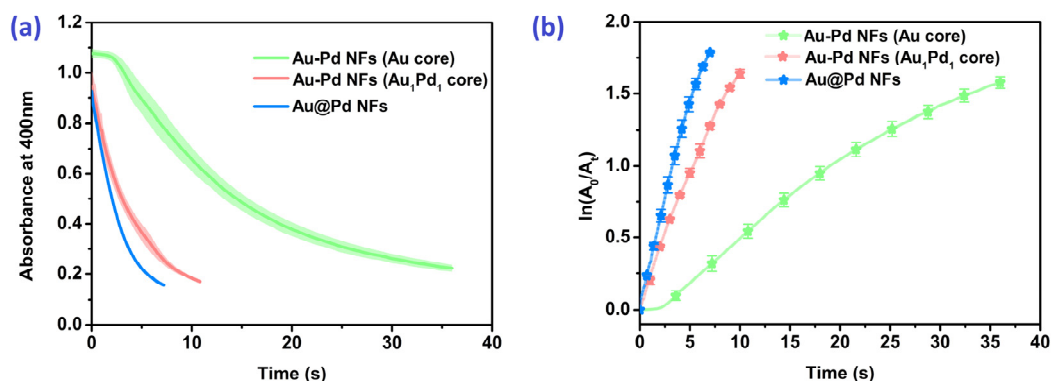
Figure 4. (**a**) The peak intensity at 400 nm for 4-NP as a function of time at room temperature in the presence of NFs. In all cases, the concentrations of 4-NP and NaBH$_4$ were 7×10^{-5} and 2.1×10^{-2} M, respectively, and the concentration of the Au-Pd catalyst was ~8 mg/L; (**b**) the relationships between $\ln(A_0/A_t)$ and the reaction time at room temperature in the presence of NFs. The error bars represent standard deviations obtained from three or more trials. These plots were then used to determine the apparent reaction rate constant (k_{app}). The absorption spectra were acquired with a UV-3600 UV-vis-NIR (ultraviolet-visible-near infrared) spectrometer (Shimadzu, Kyoto, Japan).

Au-Pd NFs (Au$_1$Pd$_1$ core, 39 nm) and Au-Pd NFs (Au core, 42 nm) manifest a much higher activity than 40 nm gold nanostars ($k_{app} = 1.78$ min^{-1}) and 40 nm gold nanospheres ($k_{app} = 0.23$ min^{-1}) [17], showing a strong synergetic effect of the high index facets and Au-Pd alloy [8]. The synergistic effect was further evidenced by increasing the Pd content of bimetallic catalyst, the activity of Au@Pd NSs increased and was able to reach more than 1.7 and 5.5 times as high as that of Au-Pd NFs (Au$_1$Pd$_1$ core) and Au-Pd NFs (Au core) with almost the same Pd content. The enhanced catalytic activity for 4-NP reduction of Au-Pd NFs (Au$_1$Pd$_1$ core), compared to Au-Pd NFs (Au core), could be attributed to more exposed reactive surfaces of Pd according to CV curves (Figure 3). Pd by alloying with gold could be favorable to the surface adsorption of the nitrophenol reactant and the reducing agent on the catalyst to follow the Langmuir-Hinshelwood mechanism, and the modification of electronic property of nanoalloys [36,37]. To better understand the synergistic effect in 4-NP reduction by Au-Pd alloy, computational calculation about the binding energy between the reactants adsorbed on the surface of the nanoalloy and the electron transfer effect between Pd and Au atoms is in progress. It is also noteworthy that the reactants could significantly change the morphology and topology of nanocatalysts [38,39], which requires specific attention in future works.

3. Materials and Methods

3.1. Synthesis of Au-Pd NFs(Au Core and Au$_1$Pd$_1$ Core)

Au-Pd NFs were prepared by a seed-mediated growth method. The seed solutions of Au and Au$_1$Pd$_1$ nanoparticles were prepared according to the reported procedures [17,20], and were then added to 29.7 mL of double distilled water under moderate stirring for 30 s. After that, 90 μL of AgNO$_3$ (10 mM), 2 mL of K$_2$PtCl$_6$ (0.5 mM) and 0.1 mL of chloroauric acid (10 mM) were added sequentially. After sufficient dispersion, 0.5 mL of ascorbic acid (0.1 M) was added to the mixture, the Au-Pd NFs (Au core) and Au-Pd NFs (Au$_1$Pd$_1$ core) were produced severally.

3.2. Synthesis of Au@Pd NFs

In a typical synthesis of Au@Pd NFs, 200 mL of HAuCl$_4$ (10 mM) was diluted with 10 mL of water, then 30 μL of AgNO$_3$ (10 mM) was added. After the resulting solution was thoroughly mixed, 40 μL of ascorbic acid (100 mM) was quickly added, and the mixture was stirred vigorously for 20 s at room temperature, then the gold multibranched nanoparticles (AuM) were produced as a seed

solution. For the subsequent growth of the Pt shell, 200 μL of K_2PtCl_6 (10 mM) was added into 10 mL of AuM colloids under stirring, followed by addition of 40 μL of ascorbic acid (100 mM). The color of the mixture changed from blue to dark gray, and Au@Pd NFs was produced.

4. Conclusions

We have developed a reproducible and facile method for the preparation of morphology-controlled Au-Pd bimetallic dendritic nanoflowers using seed mediated reduction. The prepared three NFs were characterized by UV-Vis, TEM, CV and HRTEM. The resultant Au-Pd nanodendrites exhibited a narrow size distribution and well-defined morphology, and the mass ratio of Au to Pd was able to be reduced from 18:1 to 3.5:1, detected by inductively coupled plasma optical emission spectroscopy. Three Au–Pd nanoflowers exhibited excellent catalytic activities toward the reduction of 4-NP, and the catalytic performances could be effectively tuned by varying the ratio of Au to Pd and the micro-structure of the surfaces.

Supplementary Materials: The following are available online at www.mdpi.com/2079-4991/7/9/239/s1, Figure S1: Typical transmission electron microscopy (TEM) images of synthesized seeds in this work.

Author Contributions: T.M. and F.L. conceived and designed the experiments; T.M. performed the experiments; T.M. and F.L. analyzed the data; R.C., S.L. and H.Z. contributed reagents/materials/analysis tools; T.M. and F.L. wrote the paper.

Conflicts of Interest: The authors declare no conflict of interest.

References

1. Haruta, M.; Kobayashi, T.; Sano, H.; Yamada, N. Novel gold catalysts for the oxidation of carbon monoxide at a temperature far below 0 °C. *Chem. Lett.* **1987**, *16*, 405–408. [CrossRef]

2. Haruta, M. Chance and necessity: My encounter with gold catalysts. *Angew. Chem. Int. Ed.* **2014**, *53*, 52–56. [CrossRef] [PubMed]

3. Daniel, M.C.; Astruc, D. Gold nanoparticles: Assembly, supramolecular chemistry, quantum-size-related properties, and applications toward biology, catalysis, and nanotechnology. *Chem. Rev.* **2004**, *104*, 293–346. [CrossRef]

4. Fang, J.; Zhang, B.; Yao, Q.; Yang, Y.; Xie, J.; Yan, N. Recent advances in the synthesis and catalytic applications of ligand-protected, atomically precise metal nanoclusters. *Coord. Chem. Rev.* **2016**, *322*, 1–29. [CrossRef]

5. Yu, W.; Porosoff, M.D.; Chen, J.G. Review of Pt-based bimetallic catalysis: From model surfaces to supported catalysts. *Chem. Rev.* **2012**, *112*, 5780–5817. [CrossRef] [PubMed]

6. Wang, J.; Gu, H. Novel Metal nanomaterials and their catalytic applications. *Molecules* **2015**, *20*, 17070–17092. [CrossRef] [PubMed]

7. De, S.; Zhang, J.; Luque, R.; Yan, N. Ni-based bimetallic heterogeneous catalysts for energy and environmental applications. *Energy Environ. Sci.* **2016**, *9*, 3314–3347. [CrossRef]

8. Gilroy, K.D.; Ruditskiy, A.; Peng, H.C.; Qin, D.; Xia, Y. Bimetallic nanocrystals: Syntheses, properties, and applications. *Chem. Rev.* **2016**, *116*, 10414–10472. [CrossRef] [PubMed]

9. Yan, Y.; Du, J.S.; Gilroy, K.D.; Yang, D.; Xia, Y.; Zhang, H. Intermetallic nanocrystals: Syntheses and catalytic applications. *Adv. Mater.* **2017**, *29*. [CrossRef] [PubMed]

10. Gao, F.; Goodman, D.W. Pd-Au bimetallic catalysts: Understanding alloy effects from planar models and (supported) nanoparticles. *Chem. Soc. Rev.* **2012**, *41*, 8009–8020. [CrossRef] [PubMed]

11. Weiner, R.G.; Kunz, M.R.; Skrabalak, S.E. Seeding a new kind of garden: Synthesis of architecturally defined multimetallic nanostructures by seed-mediated co-reduction. *Acc. Chem. Res.* **2015**, *48*, 2688–2695. [CrossRef] [PubMed]

12. Alshammari, A.; Kalevaru, V.N.; Martin, A. Bimetallic catalysts containing gold and palladium for environmentally important reactions. *Catalysts* **2016**, *6*, 97. [CrossRef]

13. Guerrero-Martínez, A.; Barbosa, S.; Pastoriza-Santos, I.; Liz-Marzán, L.M. Nanostars shine bright for you: Colloidal synthesis, properties and applications of branched metallic nanoparticles. *Curr. Opin. Colloid Interface Sci.* **2011**, *16*, 118–127. [CrossRef]

14. Mahmoud, M.A.; Narayanan, R.; El-Sayed, M.A. Enhancing colloidal metallic nanocatalysis: Sharp edges and corners for solid nanoparticles and cage effect for hollow ones. *Acc. Chem. Res.* **2013**, *46*, 1795–1805. [CrossRef]

15. Mahmoud, M.A.; Garlyyev, B.; El-Sayed, M.A. Controlling the catalytic efficiency on the surface of hollow gold nanoparticles by introducing an inner thin layer of platinum or palladium. *J. Phys. Chem. Lett.* **2014**, *5*, 4088–4094. [CrossRef] [PubMed]

16. Soetan, N.; Zarick, H.F.; Banks, C.; Webb, J.A.; Libson, G.; Coppola, A.; Bardhan, R. Morphology-directed catalysis with branched gold nanoantennas. *J. Phys. Chem. C* **2016**, *120*, 10320–10327. [CrossRef]

17. Ma, T.; Yang, W.; Liu, S.; Zhang, H.; Liang, F. A comparison reduction of 4-nitrophenol by gold nanospheres and gold nanostars. *Catalysts* **2017**, *7*, 38. [CrossRef]

18. Downing, R.S.; Kunkeler, P.J.; Bekkum, H.V. Catalytic syntheses of aromatic amines. *Catal. Today* **1997**, *37*, 121–136. [CrossRef]

19. Zhao, P.; Feng, X.; Huang, D.; Yang, G.; Astruc, D. Basic concepts and recent advances in nitrophenol reduction by gold- and other transition metal nanoparticles. *Coord. Chem. Rev.* **2015**, *287*, 114–136. [CrossRef]

20. Lee, Y.W.; Kim, M.; Kim, Y.; Kang, S.W.; Lee, J.H.; Han, S.W. Synthesis and electrocatalytic activity of Au-Pd alloy nanodendrites for ethanol oxidation. *J. Phys. Chem. C* **2010**, *114*, 7689–7693. [CrossRef]

21. Han, Y.; Yang, X.; Liu, Y.; Ai, Q.; Liu, S.; Sun, C.; Liang, F. Supramolecular controlled cargo release via near infrared tunable cucurbit[7]uril-gold nanostars. *Sci. Rep.* **2016**, *6*, 22239. [CrossRef] [PubMed]

22. Lim, B.; Kobayashi, H.; Yu, T.; Wang, J.; Kim, M.J.; Li, Z.Y.; Rycenga, M.; Xia, Y. Synthesis of Pd-Au bimetallic nanocrystals via controlled overgrowth. *J. Am. Chem. Soc.* **2010**, *132*, 2506–2507. [CrossRef] [PubMed]

23. Wang, L.; Huang, L.; Jiao, C.; Huang, Z.; Liang, F.; Liu, S.; Wang, Y.; Zhang, H. Preparation of Rh/Ni bimetallic nanoparticles and their catalytic activities for hydrogen generation from hydrolysis of KBH$_4$. *Catalysts* **2017**, *7*, 125. [CrossRef]

24. Zhu, X.; Jia, H.; Zhu, X.M.; Cheng, S.; Zhuo, X.; Qin, F.; Yang, Z.; Wang, J. Selective Pd deposition on Au nanobipyramids and Pd site-dependent plasmonic photocatalytic activity. *Adv. Funct. Mater.* **2017**, *27*, 1700016. [CrossRef]

25. Srisombat, L.; Nonkumwong, J.; Suwannarat, K.; Kuntalue, B.; Ananta, S. Simple preparation Au/Pd core/shell nanoparticles for 4-nitrophenol reduction. *Colloid Surf. A Physicochem. Eng. Asp.* **2017**, *512*, 17–25. [CrossRef]

26. Wang, J.; Chen, F.; Jin, Y.; Lei, Y.; Johnston, R.L. One-pot synthesis of dealloyed AuNi nanodendrite as a bifunctional electrocatalyst for oxygen reduction and borohydride oxidation reaction. *Adv. Funct. Mater.* **2017**, *27*, 1700260. [CrossRef]

27. Pan, W.; Zhang, X.; Ma, H.; Zhang, J. Electrochemical synthesis, voltammetric behavior, and electrocatalytic activity of Pd nanoparticles. *J. Phys. Chem. C* **2008**, *112*, 2456–2461. [CrossRef]

28. Han, J.; Zhou, Z.; Yin, Y.; Luo, X.; Li, J.; Zhang, H.; Yang, B. One-pot, seedless synthesis of flowerlike Au–Pd bimetallic nanoparticles with core-shell-like structure via sodium citrate coreduction of metal ions. *CrystEngComm* **2012**, *14*, 7036–7042. [CrossRef]

29. Zhang, J.; Hou, C.; Huang, H.; Zhang, L.; Jiang, Z.; Chen, G.; Jia, Y.; Kuang, Q.; Xie, Z.; Zheng, L. Surfactant-concentration-dependent shape evolution of Au-Pd alloy nanocrystals from rhombic dodecahedron to trisoctahedron and hexoctahedron. *Small* **2013**, *9*, 538–544. [CrossRef] [PubMed]

30. Yuan, H.; Khoury, C.G.; Hwang, H.; Wilson, C.M.; Grant, G.A.; Vo-Dinh, T. Gold nanostars: Surfactant-free synthesis, 3D modelling, and two-photon photoluminescence imaging. *Nanotechnology* **2012**, *23*, 075102. [CrossRef] [PubMed]

31. Zhu, C.; Zeng, J.; Tao, J.; Johnson, M.C.; Schmidt-Krey, I.; Blubaugh, L.; Zhu, Y.; Gu, Z.; Xia, Y. Kinetically controlled overgrowth of Ag or Au on Pd nanocrystal seeds: From hybrid dimers to nonconcentric and concentric bimetallic nanocrystals. *J. Am. Chem. Soc.* **2012**, *134*, 15822–15831. [CrossRef] [PubMed]

32. Óvári, L.; Bugyi, L.; Majzik, Z.; Berkó, A.; Kiss, J. Surface structure and composition of Au-Rh bimetallic nanoclusters on TiO$_2$(110): A LEIS and STM study. *J. Phys. Chem. C* **2008**, *112*, 18011–18016. [CrossRef]

33. Óvári, L.; Berkó, A.; Balázs, N.; Majzik, Z.; Kiss, J. Formation of Rh-Au core-shell nanoparticles on TiO$_2$(110) surface studied by STM and LEIS. *Langmuir* **2010**, *26*, 2167–2175. [CrossRef] [PubMed]

34. Chen, M.S.; Luo, K.; Wei, T.; Yan, Z.; Kumar, D.; Yi, C.W.; Goodman, D.W. The nature of the active site for vinyl acetate synthesis over Pd-Au. *Catal. Today* **2006**, *117*, 37–45. [CrossRef]

35. Yudanov, I.V.; Neyman, K.M. Stabilization of Au at edges of bimetallic PdAu nanocrystallites. *Phys. Chem. Chem. Phys.* **2010**, *12*, 5094–5100. [CrossRef]

36. Wunder, S.; Polzer, F.; Lu, Y.; Mei, Y.; Ballauff, M. Kinetic analysis of catalytic reduction of 4-nitrophenol by metallic nanoparticles immobilized in spherical polyelectrolyte brushes. *J. Phys. Chem. C* **2010**, *114*, 8814–8820. [CrossRef]

37. Bingwa, N.; Patala, R.; Noh, J.H.; Ndolomingo, M.J.; Tetyana, S.; Bewana, S.; Meijboom, R. Synergistic effects of gold-palladium nanoalloys and reducible supports on the catalytic reduction of 4-nitrophenol. *Langmuir* **2017**, *33*, 7086–7095. [CrossRef] [PubMed]

38. Gao, F.; Wang, Y.; Goodman, D.W. Reaction kinetics and Polarization-Modulation Infrared Reflection Absorption Spectroscopy (PM-IRAS) investigation of CO oxidation over supported Pd-Au alloy catalysts. *J. Phys. Chem. C* **2010**, *114*, 4036–4043. [CrossRef]

39. Kiss, J.; Óvári, L.; Oszkó, A.; Pótári, G.; Tóth, M.; Baán, K.; Erdóhelyi, A. Structure and reactivity of Au-Rh bimetallic clusters on titanate nanowires, nanotubes and TiO_2(110). *Catal. Today* **2012**, *181*, 163–170. [CrossRef]